

An atomistic model of electronic polarizability for calculation of Raman scattering from large-scale MD simulations

Atanu Paul¹, Anthony Ruffino³, Stefan Masiuk², Jonathan Spanier^{2,3}, and Ilya Grinberg^{1*}

¹*Department of Chemistry, Bar-Ilan University, Ramat Gan 5290002, Israel*

²*Department of Mechanical Engineering and Mechanics,*

Drexel University, Philadelphia, Pennsylvania 19104, USA and

³*Department of Physics, Drexel University, Philadelphia, Pennsylvania 19104, USA*

The application of molecular dynamics (MD) simulations to the interpretation of Raman scattering spectra is hindered by inability of atomistic simulations to account for the dynamic evolution of electronic polarizability, requiring the use of either *ab initio* method or parameterization of machine learning models. More broadly, the dynamic evolution of electronic-structure-derived properties cannot be treated by the current atomistic models. Here, we report a simple, physically-based atomistic model with few (maximum 10 parameters for the systems considered here) adjustable parameters that can accurately represent the changes in the electronic polarizability tensor for molecules and solid-state systems. Due to its compactness, the model can be applied for simulations of Raman spectra of large ($\sim 1,000,000$ -atom) systems with modest computational cost. To demonstrate its accuracy, the model is applied to the CO₂ molecule, water clusters, and BaTiO₃ and CsPbBr₃ perovskites and shows good agreement with *ab-initio*-derived and experimental polarizability tensor and Raman data. The atomistic nature of the model enables local analysis of the contributions to Raman spectra, paving the way for the application of MD simulations for the interpretation of Raman spectroscopy results. Furthermore, our successful atomistic representation of the evolution of electronic polarizability suggests that the evolution of electronic structure and its derivative properties can be represented by atomistic models, opening up the possibility of studies of electronic-structure-dependent properties using large-scale atomistic simulations.

Raman scattering spectroscopy is a powerful tool for the study of structure and dynamics of solid, liquid and gas-phase materials [1, 2]. Similar to infrared (IR) spectra, the interpretation of Raman spectra can benefit strongly from the use of molecular dynamics (MD) simulations that allow the decomposition of the total Raman spectrum into the contributions of individual modes or structural features [3]. However, since the Raman spectrum must be obtained from MD simulations using the Fourier transform of the electronic polarizability tensor time autocorrelation function [4], the derivation of Raman spectra from MD simulations requires the calculation of electronic polarizability for each time step in the MD simulation. While electronic polarizability can be calculated using density functional perturbation theory (DFPT) [5], such calculations are suitable only for simulations of small systems and short simulation times.

Several approaches have been used to circumvent this difficulty by creating models for estimating the electronic polarizability without full *ab initio* calculations. The bond-polarizability model expresses the changes in the polarizability contribution of a bond as a function of the bond lengths assuming the absence of interactions between the bonds and has been successfully used to reproduce Raman spectra of selected molecules and nanotubes [6–8]. However, this method is challenging to use in solids, where multi-atom bonding is important. Recently, an efficient method has been proposed to calculate spectra for large solids with impurities and alloys [9, 10] based on the projection of dynamics on the Raman active modes. While applicable to large systems, this method

is based on the first-order Raman scattering and therefore considers phonons around the Γ point only, which is incomplete for systems such as Si, SrTiO₃, and MoS₂ [11–13].

Alternatively, the polarizability surface (i.e. polarizability as a function of atomic coordinates) can be modeled using either polynomial expansion or deep learning methods to enable direct calculation of Raman spectra from MD trajectories [14–16]. However, both of these approaches require a large database of training structure for the parameterization of the model. Deep learning models are also more computationally expensive (by a factor of up to 100) than atomistic potentials [17–20]. However, atomistic models for polarizability similar in spirit to the atomistic models for evaluation of energy and forces from atomic coordinates have not been reported to date for complex systems with multi-center bonding. This is may be due to the assumption that the response of electronic structure to the incident electromagnetic field and its dependence on atomic coordinates in a solid-state material are too complicated to be decomposed into contributions of individual atoms and expressed by a simple atomistic model and thus can only be modeled using quantum mechanical approaches.

Here, we demonstrate that by considering the effect of the dynamical changes in the structure and chemical bonding in molecules or materials together with the second-order perturbation theory expression for electronic polarizability, a computationally efficient and atomistically-interpretable model with few adjustable parameters characterizing the evolution of electronic polar-

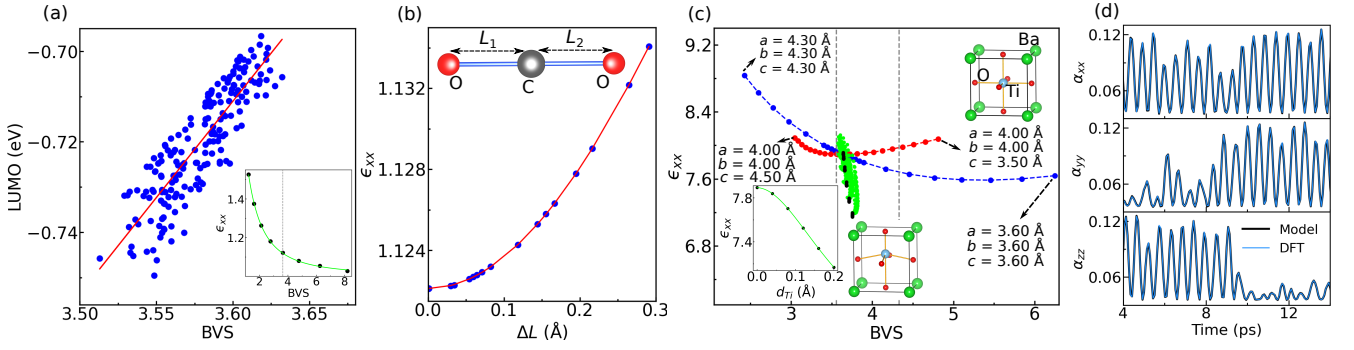


FIG. 1. (Color online) (a) LUMO (eV) vs BVS (blue circles) and the linear fit (red line) for CO₂ structures generated by MD at 300 K. Inset: the Lorentzian function fit (green) of ϵ_{xx} to BVS (black dots) for symmetrically stretched CO₂. Gray dotted line (Inset): BVS (3.64) of CO₂ at DFT-relaxed position. (b) ϵ_{xx} vs ΔL ($|L_1 - L_2|$) for CO₂ for BVS = 3.64 (blue circles) with the Lorentzian fit (red). L_1 and L_2 are C-O bond lengths (see inset). (c) ϵ_{xx} vs Ti BVS for five-atom BTO for isotropic volume change of cubic centrosymmetric BTO (blue), compression and extension of the z -axis of centrosymmetric BTO (red), Ba and Ti shifted along x -direction while O are fixed at centrosymmetric positions for cubic BTO with $a = 4.00$ Å (black circles), Ba and Ti fixed at the centrosymmetric positions while O are shifted along x -direction for cubic BTO with $a = 4.00$ Å (green circles). Gray dotted lines: Minimum (3.56) and maximum (4.33) Ti BVS from 5-atom MD in the temperature range 200-1000 K. Bottom corner inset: Lorentzian fit (green) of ϵ_{xx} vs off-centre displacement of Ti (d_{Ti} (Å)) (black dots), where Ba and O are at centrosymmetric position. (d) Polarizability (α_{xx} , α_{yy} and α_{zz}) trajectory using model and DFT for CO₂ at 300 K.

izability in terms of atomic coordinates can be derived. We then apply the model with ≤ 10 parameters for the calculation of Raman spectra from MD simulations using CO₂, water clusters ((H₂O)_{*n*}: $n = 1-6, 8$), and BaTiO₃ (BTO) and CsPbBr₃ (CPB) systems with supercells of up to $\approx 500,000$ atoms to demonstrate the accuracy of this approach.

From perturbation theory, the polarizability tensor (α) can be represented as [21, 22]

$$\alpha_{ij} \propto \sum_{\gamma \neq 0} \frac{\langle \Phi_0 | \hat{p}_i | \Phi_\gamma \rangle \langle \Phi_\gamma | \hat{p}_j | \Phi_0 \rangle}{\hbar(\omega_\gamma - \omega_0)}$$

where $|\Phi_0\rangle$ and $|\Phi_\gamma\rangle$ are ground and excited states, \hat{p}_i is the induced electric dipole operator due to external field, and $\hbar(\omega_\gamma - \omega_0)$ is the energy difference between excited and ground states. Thus, the atomistic model must take into account the effect of the changes of the bonding and the coupling between the individual bonds on this perturbation theory expression. The denominator ($\omega_\gamma - \omega_0$) can be related to the second moment of the local density of states and thus the bond valence sum (BVS) [23, 24] defined as

$$\text{BVS} = \sum_i \exp((d_{AB}^0 - d_i)/b) \quad (1)$$

where d_{AB}^0 and d_i are the bond valence parameter and bond length for the bond between atoms A and B , respectively, b ($= 0.37$ Å) is an universal constant [25]. Therefore, BVS rather than the individual bond lengths characterizes the changes in the local bonding environment and should be related to the α . We use the CO₂ molecule

as a simple model system to demonstrate the relationship between BVS and the LUMO energy (see Fig. 1 (a)). Plotting ϵ versus BVS for a symmetric stretching of CO₂, we find that the atom's polarizability (α) due to symmetrically stretched bond can be characterized by Lorentzian function of the BVS of that atom (see inset of Fig. 1 (a)) [26].

Since BVS is insensitive to the details of the local atomic arrangement, the effect of local asymmetry on α must be taken into account separately. We investigate the influence of the asymmetry on α by plotting ϵ_{xx} versus the bond length difference (ΔL) in CO₂ for a fixed BVS (3.64) so that the values of $(\omega_\gamma - \omega_0)$ show only small variation (Fig. 1 (b)). It is observed that α shows a Lorentzian dependence on the asymmetry of CO₂.

To understand the relationship between α and atomic coordinates, BVS and asymmetry in a more complicated solid-state system, we considered the following cases for a 5-atom BTO cell: (a) isotropic volume change of cubic centrosymmetric BTO, (b) Ba and Ti displacing along x direction and O fixed at centrosymmetric position for cubic BTO where lattice constant = 4.00 Å and (c) Ba and Ti fixed at the centrosymmetric positions and O displacing along x direction for cubic BTO where lattice constant = 4.00 Å, (d) Anisotropic volume change (tetragonal distortion) of centrosymmetric BTO. The plots of α versus Ti BVS for cases (a)-(d) are shown in Fig. 1 (c). For (a), we observed a Lorentzian dependence of α on BVS in the physically relevant range of $\approx 3.5-4.5$. For (b) and (c), despite the small variation in BVS, a strong change in α is observed with α decreasing strongly with greater off-center atomic displacement (asymmetry). The dependence of α on asymmetry (off-center dis-

placement of Ti) also follows a Lorentzian dependence (see inset of Fig. 1 (c)). For (d), we observe an interesting trend of α first decreasing and then increasing with the change in the BTO aspect ratio. The results for cases (a)-(c) show that similar to the CO₂ molecule, α for the solid-state BTO shows Lorentzian dependence on the BVS and the asymmetric atomic displacement. The results for (d) can be explained by considering that more isolated atoms have higher α than the corresponding more bonded system (in part due to lower $(\omega_\gamma - \omega_0)$) and that BTO with either very low or very high aspect ratio will contain O atoms (axial O atoms for high aspect ratio, equatorial O atoms for low aspect ratio) that participate only weakly in bonds with Ti. For high aspect ratio, the long distances between Ti and axial O atoms will make the O atoms more non-bonding and will increase α . For low aspect ratio, the very short distances between Ti and axial O atoms will lead to the concentration of the bonding along the z -axis, leaving the O atoms in the xy plane with weak bonds to Ti even for the Ti-O distances of 2.0 Å. To represent this effect, we introduce dynamical charge m for evaluation of the actual bond order of a given Ti-O bond taking into account the competition for bonding charge with all other bond.

Based on the insights obtained from the relationships described above, we define the bond polarizability α_{ij} between atoms A and B where sum over bond polarizability gives total α , as

$$\begin{aligned} \alpha_{ij} = & [A_{\parallel}^s * A_{\parallel}^a + B_{\parallel}^s * B_{\parallel}^a] * \left(\frac{R_i R_j}{R^2} \right) \\ & + [A_{\perp}^s * A_{\perp}^a + B_{\perp}^s * B_{\perp}^a] * \left(\delta_{ij} - \frac{R_i R_j}{R^2} \right) \end{aligned} \quad (2)$$

where dielectric constant (ϵ_{ij}) is related to α_{ij} as, $\alpha_{ij} \propto (\epsilon_{ij} - \delta_{ij})$. Here i, j denote x, y or z axes. The first and second expression of α_{ij} give the parallel and perpendicular contribution of the bond to α_{ij} , respectively. A_{\parallel}^s (B_{\parallel}^s) and A_{\parallel}^a (B_{\parallel}^a) describe the effects of the symmetric and asymmetric bond length changes on the contribution of A (B) ion to the polarizability along the $A - B$ bond direction. Similarly, A_{\perp}^s (B_{\perp}^s) and A_{\perp}^a (B_{\perp}^a) describe the effects of the symmetric and asymmetric bond length changes on the contribution of A (B) ion to the polarizability perpendicular to the $A - B$ bond direction. Here R defines the $A - B$ bond length. $\delta_{ij} = 1$ if $i = j$ and $\delta_{ij} = 0$ if $i \neq j$, following the approach developed for the bond polarizability model [8].

We define $A_{\parallel}^s, A_{\parallel}^a, B_{\parallel}^s, B_{\parallel}^a, A_{\perp}^s, A_{\perp}^a, B_{\perp}^s$ and B_{\perp}^a using a simple Lorentzian function. Thus we have the following expressions,

$$\begin{aligned} A_{\parallel}^s &= \frac{a_1^2}{(x_A^s - a_2)^2 + a_3^2}, B_{\parallel}^s = \frac{a_1^2}{(x_B^s - a_2)^2 + a_3^2}, A_{\perp}^s = \frac{a_8^2}{(y_{A,\perp}^s)^2 + a_8^2} \\ A_{\perp}^a &= \frac{a_4^2}{(x_A^a - a_5)^2 + a_6^2}, B_{\perp}^a = \frac{a_4^2}{(x_B^a - a_5)^2 + a_6^2}, B_{\perp}^s = \frac{a_{10}^2}{(y_{B,\perp}^s)^2 + a_{10}^2} \\ A_{\parallel}^a &= \frac{a_7^2}{(y_{A,\parallel}^a)^2 + a_7^2}, B_{\parallel}^a = \frac{a_9^2}{(y_{B,\parallel}^a)^2 + a_9^2} \end{aligned}$$

In the above expressions $a_1, a_2, a_3, a_4, a_5, a_6, a_7, a_8,$

$a_9,$ and a_{10} , are the constants in the Lorentzian expressions to be fit to DFPT-calculated polarizability data. x_A^s, x_B^s, y_A^a and y_B^a are determined from the atomic coordinates. x_A^s is defined as, $x_A^s = BVS \times \frac{m}{m_0}$ here BVS = total bond valence of A given by Eq. 1, m is the dynamical formal charge of A ion that varies depending on the environment, and m_0 is the formal charge of A (e.g. 4 for C and Ti in CO₂ and BTO and 2 for O). The dynamical charge state is defined as, $m = \sum_k [\frac{BV_k}{BVS_k} \times m_{0k}]$. Here, k is the neighbor bond index of A . BV_k is the bond valence of the k -th $A-B$ bond. BVS_k and m_{0k} are the total bond valence and formal charge of B ion residing at k -th $A-B$ bond, respectively. $x_{s,B}$ is defined in similar manner to $x_{s,A}$.

Then, y_A^a is the asymmetric displacement of A ion from the center of mass of the nearest-neighbor B ions. $y_{A,\parallel}^a$ and $y_{A,\perp}^a$ are the parallel and perpendicular projection of the asymmetric displacement on the $A-B$ bond. y_B^a is the asymmetric displacement of B ion from the center of mass of the nearest-neighbor A ions. $y_{B,\parallel}^a$ and $y_{B,\perp}^a$ are defined similarly to $y_{A,\parallel}^a$ and $y_{A,\perp}^a$.

To calculate these unknown parameters of Lorentzian expressions, we first calculated polarizability trajectory (α_{DFT}) from density functional theory (DFT) for a small number of points along the MD trajectory. We then optimized the parameters in the our model for α_{ij} (Eq. 2) to reproduce the α_{DFT} using simulated annealing algorithm, with the optimized parameters given in SM. A comparison between the DFT α trajectories and the model α trajectories for CO₂ are presented in Fig. 1 (d), showing excellent agreement.

Next, we apply our model to calculate Raman spectra of water clusters $((\text{H}_2\text{O})_n: n = 1-6, 8)$. Fig. 2 (a) show the comparison of polarizability (α_{xx}) trajectory at 300 K as calculated from DFT and the model for H₂O. Clearly, the model trajectory captured the main features of the DFT trajectory. We then calculate the Raman spectra of H₂O from the atomic coordinates obtained from MD simulations, with the results shown in Fig. 2 (b)(First panel). The spectrum calculated from the DFT-obtained polarizability time autocorrelation function as shown in the same plot gives a good agreement between them. The spectra consist of three peaks, corresponding to the H-O-H bending mode (the small peak around 1600 cm⁻¹), and the symmetric and asymmetric O-H stretching modes at around 3800 cm⁻¹ and 3900 cm⁻¹ respectively. These results are in agreement with available experimental Raman spectra [27]. To examine whether our model can be used to capture the effects of hydrogen bonding on Raman spectra, we compared the DFT and model Raman spectra of (H₂O)₂ and (H₂O)₃ clusters as calculated using the same constants as those used for single H₂O (see Fig. 2(b)), which also show a good agreement between model and DFT results. This shows that the model can handle systems with hydrogen-bonded water because the effect of hydrogen bonding on

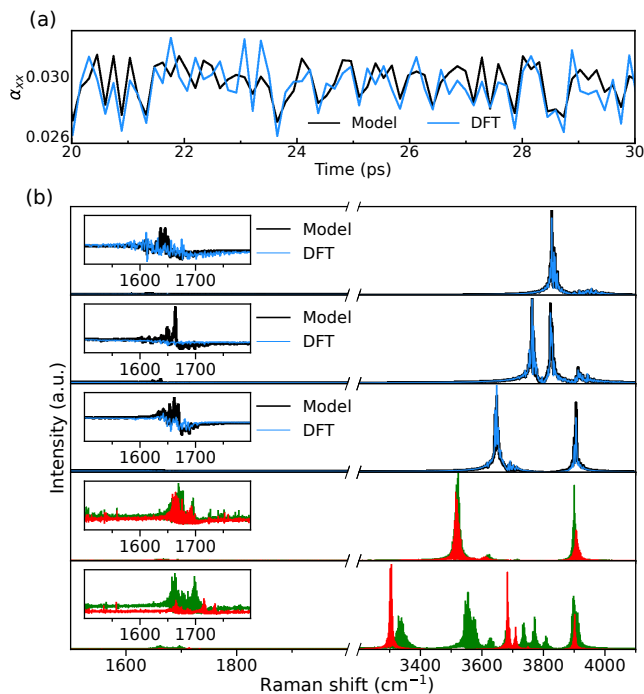


FIG. 2. (Color online) (a) Polarizability (α_{xx}) trajectory from model and DFT for H_2O molecule at 300 K. (b) Raman spectra of H_2O clusters ($(\text{H}_2\text{O})_n$; $n = 1-6, 8$). First, second and third panels show spectra of H_2O , $(\text{H}_2\text{O})_2$ and $(\text{H}_2\text{O})_3$ from model and DFT respectively. Fourth panel: model spectra for $(\text{H}_2\text{O})_4$ (green) and $(\text{H}_2\text{O})_5$ (red). Fifth panel: model spectra for $(\text{H}_2\text{O})_6$ (green) and $(\text{H}_2\text{O})_8$ (red).

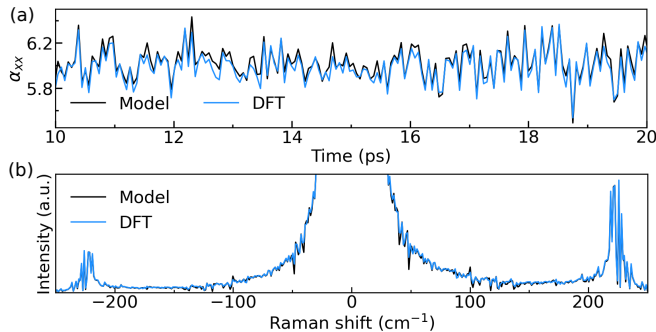


FIG. 3. (Color online) (a) Polarizability (α_{xx}) trajectory, (b) Raman spectra from model and DFT for BaTiO_3 (5 atoms cell) at 300 K.

polarizability is mostly due to the changes of the H_2O geometry induced by hydrogen bonds, whereas hydrogen bonds induce only small changes in the response of the electron cloud to electric field for a given H_2O geometry. Due to the computational constraints, the above-discussed DFT-derived spectra were obtained for runs of 44 ps with a time step of 0.003 ps and the same simulation duration and time step and trajectories were also used for the calculation of model-derived spectra. In the SM, we present the more accurate model Raman spectra

of H_2O , $(\text{H}_2\text{O})_2$ and $(\text{H}_2\text{O})_3$ derived from atomistic ([28–30]) simulation trajectories for 3 ns with a time step of 0.001 ps. We have also calculated the Raman spectra for $(\text{H}_2\text{O})_4$, $(\text{H}_2\text{O})_5$, $(\text{H}_2\text{O})_6$ and $(\text{H}_2\text{O})_8$ using the longer atomistic potential trajectories as shown in the fourth and fifth panels of Fig. 2(b), respectively. The peak positions of the $(\text{H}_2\text{O})_n$, $n = 1-6, 8$ are in good agreement with the results in the literature [30].

Next we apply the model to the classic ferroelectric BTO for which an atomistic potential is available [31], enabling large MD simulations. We use the *ab initio* MD α data as calculated using 10-atom BTO cell to fit the parameters in Eq. 2 for the TiO_6 octahedron only. We ignore the contribution of the BaO_{12} polyhedra to α because it is small relative to that of TiO_6 due to predominantly Ti 3d character of the conduction band (see the SM for more information). In Fig. 3 (a), we present the trajectories of α_{xx} at 300 K as calculated using DFT and the parameterized model, respectively. It is observed here as well that the model α_{xx} trajectory is in good agreement with the DFT trajectory. For direct comparison of the model with DFT results, we calculated Raman spectra using DFT α_{xx} and model α_{xx} with the results shown in Fig. 3 (b) [32]. The figure shows that the DFT-based and model-based spectra are in good agreement.

Next, we considered a large simulation cell of single-domain BTO with the dimensions of $16 \times 16 \times 16$ (20,480 atoms) in order to examine the accuracy of the model in characterizing the phase transition of BTO. We calculated the trajectories using atomistic MD with the bond-valence potential for different temperature between 10 K and 160 K which capture all of the phases of BTO for this potential [33]. The evolution of polarization with time for all of these phases is presented in the SM. We then used the same constants as obtained for 10-atom BTO cell to calculate the Raman spectra of the single-domain $16 \times 16 \times 16$ BTO for all the considered temperatures. Fig. 4 compares the results obtained by our model calculations with the experimentally obtained spectra of single-crystal BTO (see SM also). Examination of the theoretical Raman spectra shows that rhombohedral, orthorhombic, tetragonal and cubic phases are achieved at < 80 K, 90-95 K, 100-130 K and > 160 K, respectively. This corresponds to the experimentally observed phase transitions at 183, 278 and 393 K due to the underestimation of the phase transition temperatures by DFT-based potentials [31]. Additionally, with the increase of temperature, both experimental and theoretical spectra show peak broadening. For the rhombohedral phase at 40 K in the theoretical results, the peaks below 200 cm^{-1} match well the R-phase experimental peaks below 200 cm^{-1} . The two peaks in the range of $200-500 \text{ cm}^{-1}$ in the theoretical spectra correspond to the two peaks in the $200-400 \text{ cm}^{-1}$ in the experimental spectra. The peaks between 500 and 700 cm^{-1} in theoretical spectra correspond to the peak around 500 cm^{-1} observed ex-

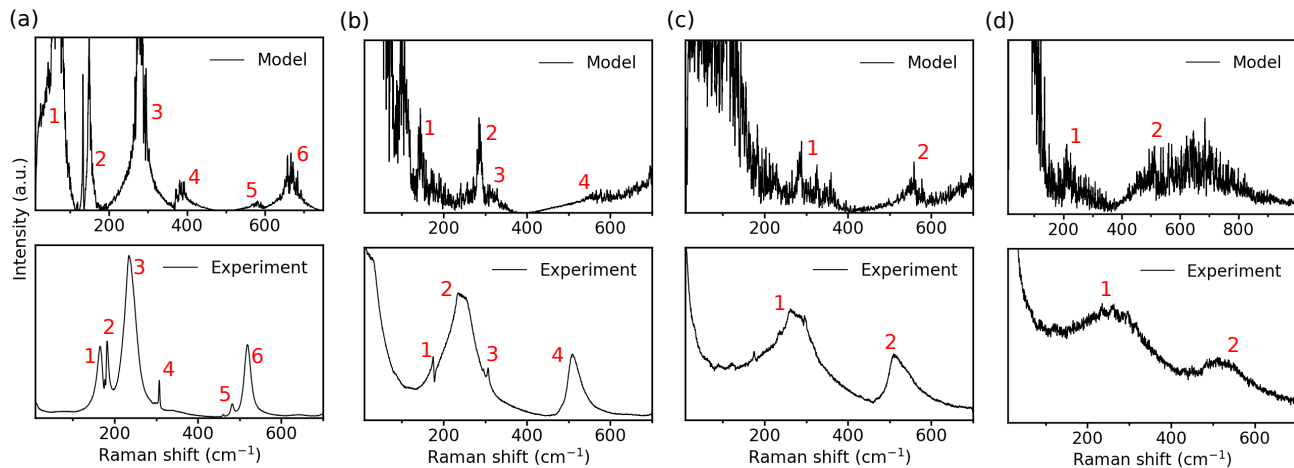


FIG. 4. (Color online) Raman spectra of single crystal BTO for different phases (a) rhombohedral, (b) orthorhombic, (c) tetragonal, and (d) cubic from model and experiment. The temperatures for (a), (b), (c) and (d) are 40, 92, 110 and 160 K respectively (top panel), and 123, 233, 333 and 423 K respectively (bottom panel).

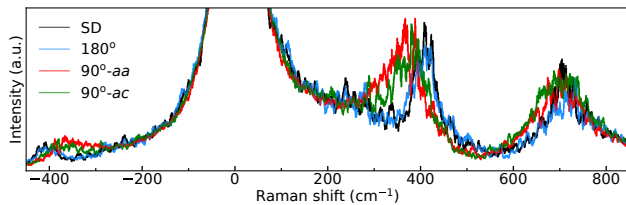


FIG. 5. (Color online) Raman spectra for different Domain structure of BTO.

perimentally. The peak in the high wavenumber region as observed theoretically (see SM) is also consistent with the experimental peak above 700 cm^{-1} [34]. Similarly, the comparison between theoretical results and experimental results shows good agreement for other phases of BTO. We also applied the model to CPB halide perovskite and obtained good agreement between DFT and model polarizability trajectories and Raman spectra (see SM).

To further demonstrate the utility of the model, we applied it to the Raman spectra of different ferroelectric domain structures of BTO to show that Raman spectra can distinguish between the different domain phases and these difference can be interpreted using the atomistic polarizability model. We considered single-domain, 180° domain, $90^\circ(aa)$ domain and $90^\circ(ac)$ domain structures of BTO based on MD simulations using $120 \times 120 \times 6$ supercell (432,000 atoms) with the obtained Raman spectra shown in Fig. 5. It is clear that different domain variants can be detected based on the differences between their respective Raman spectra. These simulations also show that Raman spectra can be obtained for large supercells at essentially negligible computational cost that is only $\sim 50\%$ of the computational cost of BV potential MD simulations. (70 CPU hours required for MD simulations

and 35 CPU hours required for each Raman spectrum calculations on 32 core machine).

To summarize, we have demonstrated that a simple, physically-based atomistic model with only 10 adjustable parameters can accurately represent the changes in the electronic polarizability of complex system such as BTO. Due its physical basis, the model is much more compact than the polynomial expansion (128 adjustable parameters for H_2O molecule [14]) and the deep-learning models of the polarizability tensor. This enables efficient calculations of Raman spectra from large-scale MD simulations with only modest computational resources as well as atomistic and local analysis of the contributions to Raman spectra for the interpretation of Raman spectroscopy results.

* ilya.grinberg@biu.ac.il

- [1] H. J. Butler, L. Ashton, B. Bird, G. Cinque, K. Curtis, J. Dorney, K. Esmonde-White, N. J. Fullwood, B. Gardner, P. L. Martin-Hirsch, M. J. Walsh, M. R. McAinsh, N. Stone, and F. L. Martin, *Nature Protocols* **11**, 664 (2016).
- [2] X. Zhang, X.-F. Qiao, W. Shi, J.-B. Wu, D.-S. Jiang, and P.-H. Tan, *Chem. Soc. Rev.* **44**, 2757 (2015).
- [3] O. Yaffe, Y. Guo, L. Z. Tan, D. A. Egger, T. Hull, C. C. Stoumpos, F. Zheng, T. F. Heinz, L. Kronik, M. G. Kanatzidis, J. S. Owen, A. M. Rappe, M. A. Pimenta, and L. E. Brus, *Phys. Rev. Lett.* **118**, 136001 (2017).
- [4] M. Thomas, M. Brehm, R. Fligg, P. Vöhringer, and B. Kirchner, *Phys. Chem. Chem. Phys.* **15**, 6608 (2013).
- [5] S. Baroni, S. de Gironcoli, A. Dal Corso, and P. Gianozzi, *Rev. Mod. Phys.* **73**, 515 (2001).
- [6] S. Guha, J. Menéndez, J. B. Page, and G. B. Adams, *Phys. Rev. B* **53**, 13106 (1996).
- [7] L. Wirtz, M. Lazzeri, F. Mauri, and A. Rubio, *Phys.*

- Rev. B **71**, 241402 (2005).
- [8] P. Hermet, N. Izard, A. Rahmani, and P. Ghosez, *The Journal of Physical Chemistry B* **110**, 24869 (2006).
- [9] A. Hashemi, A. V. Krasheninnikov, M. Puska, and H.-P. Komsa, *Phys. Rev. Mater.* **3**, 023806 (2019).
- [10] Z. Kou, A. Hashemi, M. J. Puska, A. V. Krasheninnikov, and H.-P. Komsa, *npj Computational Materials* **6**, 59 (2020).
- [11] J. H. Parker, D. W. Feldman, and M. Ashkin, *Phys. Rev.* **155**, 712 (1967).
- [12] W. G. Nilson and J. G. Skinner, *The Journal of Chemical Physics* **48**, 2240 (1968).
- [13] T. Livneh and J. E. Spanier, *2D Materials* **2**, 035003 (2015).
- [14] O. Omodemi, S. Sprouse, D. Herbert, M. Kaledin, and A. L. Kaledin, *Journal of Chemical Theory and Computation* **18**, 37 (2022).
- [15] G. M. Sommers, M. F. Calegari Andrade, L. Zhang, H. Wang, and R. Car, *Phys. Chem. Chem. Phys.* **22**, 10592 (2020).
- [16] R. Luo, J. Popp, and T. Bocklitz, *Analytica* **3**, 287 (2022).
- [17] P. Mo, C. Li, D. Zhao, Y. Zhang, M. Shi, J. Li, and J. Liu, *npj Computational Materials* **8**, 107 (2022).
- [18] J. Wu, Y. Zhang, L. Zhang, and S. Liu, *Phys. Rev. B* **103**, 024108 (2021).
- [19] L. Zhang, J. Han, H. Wang, R. Car, and W. E, *Phys. Rev. Lett.* **120**, 143001 (2018).
- [20] W. Jia, H. Wang, M. Chen, D. Lu, L. Lin, R. Car, E. Weinan, and L. Zhang, in *SC20: International Conference for High Performance Computing, Networking, Storage and Analysis* (2020) pp. 1–14.
- [21] S. Lubner, M. Iannuzzi, and J. Hutter, *The Journal of Chemical Physics* **141**, 094503 (2014).
- [22] D. A. Long, *The Raman Effect* (John Wiley & Sons, Ltd, 2002).
- [23] A. P. Sutton, *Electronic structure of materials*, Oxford science publications (Clarendon Press, Oxford, 2004 - 1993).
- [24] S. Liu, I. Grinberg, H. Takenaka, and A. M. Rappe, *Phys. Rev. B* **88**, 104102 (2013).
- [25] N. E. Brese and M. O’Keeffe, *Acta Crystallographica Section B* **47**, 192 (1991).
- [26] α_{xx} = normalization factor $\times (\epsilon_{xx} - 1)$ and the normalization factor is related to the amount of vacuum in the unit cell used to calculate ϵ_{xx} . Both of these give similar expressions. Therefore, while plotting we have shown DFT-calculated ϵ_{xx} . However, in text we always use α_{xx} .
- [27] M. H. Brooker, G. Hancock, B. C. Rice, and J. Shapter, *Journal of Raman Spectroscopy* **20**, 683 (1989).
- [28] V. Babin, G. R. Medders, and F. Paesani, *Journal of Chemical Theory and Computation* **10**, 1599 (2014).
- [29] P. Eastman, J. Swails, J. D. Chodera, R. T. McGibbon, Y. Zhao, K. A. Beauchamp, L.-P. Wang, A. C. Simmonett, M. P. Harrigan, C. D. Stern, R. P. Wiewiora, B. R. Brooks, and V. S. Pande, *bioRxiv* (2017), 10.1101/091801.
- [30] N. R. Samala and N. Agmon, *The Journal of Physical Chemistry B* **123**, 9428 (2019).
- [31] Y. Qi, S. Liu, I. Grinberg, and A. M. Rappe, *Phys. Rev. B* **94**, 134308 (2016).
- [32] Though this is not the actual spectra as we considered trajectory for small time with large time step, these results indicate the accuracy of this model.
- [33] Since the BV potential is based on DFT calculations, it underestimates the Curie temperature of BTO due to the underestimation of the O_6 rotation energy cost by DFT as shown in previous work [31].
- [34] M. Deluca, Z. G. Al-Jlaihawi, K. Reichmann, A. M. T. Bell, and A. Feteira, *J. Mater. Chem. A* **6**, 5443 (2018).

Supplemental Material: An atomistic model of electronic polarizability for calculation of Raman scattering from large-scale MD simulations

Atanu Paul¹, Anthony Ruffino³, Stefan Masiuk², Jonathan Spanier^{2,3}, and Ilya Grinberg^{1*}

¹Department of Chemistry, Bar-Ilan University, Ramat Gan 5290002, Israel

²Department of Mechanical Engineering and Mechanics,

Drexel University, Philadelphia, Pennsylvania 19104, USA and

³Department of Physics, Drexel University, Philadelphia, Pennsylvania 19104, USA

CONTENTS

Computational details	1
Experimental details	2
H ₂ O clusters	2
Importance of asymmetry and dynamical charge state (m)	2
BaTiO ₃ five atoms cell	2
BaTiO ₃ single domain and polydomain state calculations	3
CsPbBr ₃	5
CO ₂ molecule	5
Effect of BaO ₁₂ on polarizability of BTO	5
References	5

COMPUTATIONAL DETAILS

Density functional theory (DFT) as well as *ab initio* molecular dynamics (AIMD) calculations were performed using the Quantum ESPRESSO code [1] with the Perdew-Burke-Ernzerhof exchange-correlation functional for solids (PBEsol) [2] for all the systems considered here. The dielectric function was calculated within the framework of random phase approximation (RPA) as implemented in Quantum ESPRESSO. The kinetic energy cutoff for the expansion of the wave functions was set to 40 and 110 Ry for the AIMD and dielectric function calculations, respectively, for all systems.

In order to calculate the Lorentzian constants for modeling of the Raman spectra of water clusters ((H₂O)_{*n*}: *n* = 1-6, 8), we considered *n* = 1, *i.e.* H₂O molecule only. We then extracted eight constants (because the asymmetry effect is unnecessary for H atoms) after optimizing the model polarizability with respect to that obtained from DFT calculations on AIMD structures (300 structures) at 300 K. The extracted values of the Lorentzian constants are $a_1 = 0.163408$, $a_2 = -0.176637$, $a_3 = 0.640497$, $a_4 =$

-0.325206 , $a_5 = -2.420756$, $a_6 = 0.667671$, $a_7 = 2.626936$, $a_8 = 6.445961$. Those constants were used to calculate the atomistic model polarizability for other (H₂O)_{*n*} systems. Classical molecular dynamics of (H₂O)_{*n*} was performed using MB-pol [3, 4] to obtain a long trajectory of up to 3 ns with a time step of 0.001 ps, where the temperature of the dynamics were 50 K for *n* = 2 to 6, and 10 K for *n* = 1 and 8. In order to compare the model spectra with DFT spectra for H₂O, (H₂O)₂ and (H₂O)₃, a short trajectory of up to 44 ps with a time step of 0.003 ps was also considered.

The Lorentzian constants for BaTiO₃ (BTO) were extracted after optimizing the model polarizability with respect to polarizability from DFT where the structures for the DFT calculations were taken from AIMD on 10-atom BTO cell at 300 K, 600 K, 800 K and 1000 K. After optimizing the parameters to reproduce the polarizabilities of 120 structures (30 from each temperature), the extracted values were obtained as $a_1 = 1.543787$, $a_2 = 2.030938$, $a_3 = 1.635022$, $a_4 = 3.113967$, $a_5 = -0.481618$, $a_6 = 3.091547$, $a_7 = -1.060428$, $a_8 = 6.501974$, $a_9 = 0.227096$ and $a_{10} = 2.492371$. While performing the AIMD, the Brillouin zone integration was executed using $2 \times 4 \times 4$ and $4 \times 4 \times 4$ \mathbf{k} mesh for $2 \times 1 \times 1$ (10 atoms) and $1 \times 1 \times 1$ (5 atoms) cells of BTO, respectively. To calculate the polarizability tensor from DFT, we considered a larger \mathbf{k} mesh of $3 \times 6 \times 6$ and $6 \times 6 \times 6$ for the $2 \times 1 \times 1$ (10 atoms) and $1 \times 1 \times 1$ (5 atoms) cells of BTO, respectively. The classical MD simulations were performed using the LAMMPS code [5] with the atomistic potential [6] for BTO for time up to 300 ps with a time step 0.001 ps to obtain dynamics of BTO single-domain and polydomain systems. To simulate single-crystal single domain BTO, we considered a $16 \times 16 \times 16$ cell size. The dynamics of the BTO domain structures (single (SD), 180° , 90° -*aa* and 90° -*ac* domain) were investigated using the $120 \times 120 \times 6$ cells.

The constants for the Lorentzian functions in the atomistic polarizability model for CsPbBr₃ (CPB) were evaluated in a similar manner to those for BTO and were derived from AIMD and DFT results obtained for the $2 \times 1 \times 1$ (10 atoms) cell of CPB at 300 K, 600 K and 800 K. The values of the Lorentzian constants for CPB are $a_1 = -2.433495$, $a_2 = 0.799679$, $a_3 = 3.013168$, $a_4 = 1.636966$, $a_5 = 6.067340$, $a_6 = 2.496868$, $a_7 = -13.071122$, $a_8 = 9.703365$, $a_9 = 0.615866$, $a_{10} = 6.620343$. The Brillouin zone integration was executed using $2 \times 4 \times 4$ and $4 \times 4 \times 4$ \mathbf{k} mesh for $2 \times 1 \times 1$ (10 atoms) and $1 \times 1 \times 1$ (5 atoms) cells of CPB, respectively.

loun integration was performed using the similar size of k mesh as already described for BTO. In order to compare the Raman spectra from model and DFT calculation, we considered a MD trajectory of short time of 60 ps with a large time step of 0.15 ps.

To extract Lorentzian constants for CO₂, the polarizability model parameters were optimized to match the polarizability calculated by DFT for 200 structures obtained from AIMD at 300 K. The extracted Lorentzian constants for CO₂ molecule are $a_1 = 0.311722$, $a_2 = 1.067479$, $a_3 = 1.064764$, $a_4 = 0.255176$, $a_5 = 0.160768$, $a_6 = 1.316444$, $a_7 = 0.940256$ and $a_8 = 1.158281$. However, the Raman spectrum of CO₂ was calculated for a trajectory of 64 ps with a time step of 0.0014 ps as obtained from AIMD at 300 K.

It is important to note that all the extracted Lorentzian constants are not unique and may vary depending on the optimization conditions.

EXPERIMENTAL DETAILS

Inelastic light scattering (Raman scattering) was performed in the backscattering VV configuration ($Z(X, X)\bar{Z}$, $X\parallel(100)$) with a 5 mW 385 nm excitation source (M Squared Lasers) focused to a surface intensity of 1 W/cm². Light was dispersed by a T64000 triple spectrometer (Horiba Jobin-Yvon), and collected with an air-cooled CCD (Andor). The (001)-oriented BaTiO₃ bulk single crystal was grown by top seeded solution growth (MTI Corp.).

Raman spectra were collected between 123 K and 423 K at 5 K intervals, and each individual spectrum is 3 averaged acquisitions of 10 seconds. Experimental observations of abrupt structural phase transitions at 183 K (R to O), 278 K (O to T), and 393 K (T to C) are in agreement with existing literature on the material. Additionally, the intensity of the collapsing soft mode (160 cm⁻¹ in R-phase, and the broad feature at 35 cm⁻¹ in O-phase) are an indication of structural homogeneity and a low population of domain walls, showing these are effectively single-domain measurements.

H₂O CLUSTERS

The Raman spectra from model and DFT for the cases of $n = 1, 2$ and 3 using short trajectory are already presented in the main paper. In Fig. S1 (a), (b), (c), we plot the Raman spectra again but using long trajectory of 3 ns and smaller time step of 0.001 ps along with the spectra obtained using the short trajectory for $n = 1, 2$ and 3 . The long trajectory clearly also find the similar peak position as obtained using short trajectory.

IMPORTANCE OF ASYMMETRY AND DYNAMICAL CHARGE STATE (m)

The expression for the polarizability (Eq. 2 of the main paper) is composed of symmetric and asymmetric parts where the symmetric part also contain the dynamical charge state (m). In this section, the importance of each term for the calculation of the spectra is examined. We considered BTO and evaluate the polarizability as well as Raman spectra with the model for the following four cases: (a) the effects of both asymmetry and m are included, (b) the effect of asymmetry is not included but the effect of m is included, (c) the effect of asymmetry is included but the effect of m is not included, (d) the effects of both asymmetry and m are not included. The Lorentzian constants for case (a) are already presented in the ‘COMPUTATIONAL DETAILS’ section. The extracted Lorentzian constants for the other cases are (b) $a_1 = -3.411483$, $a_2 = -1.503017$, $a_3 = 1.392625$, $a_4 = 1.976437$, $a_5 = -1.092110$, $a_6 = 0.932035$, (c) $a_1 = 1.228825$, $a_2 = 2.203616$, $a_3 = 1.089328$, $a_4 = 2.380694$, $a_5 = 0.003688$, $a_6 = 2.304688$, $a_7 = -2.924001$, $a_8 = 3.447771$, $a_9 = 0.243666$, $a_{10} = 2.528604$, (d) $a_1 = -2.236458$, $a_2 = -0.183282$, $a_3 = 1.235218$, $a_4 = 1.469221$, $a_5 = -0.336989$, $a_6 = 0.944660$. Fig. S2 represents the polarizability trajectory calculated from the model for the four cases along with the DFT trajectory for five-atom BTO at 300 K. For all cases, the model trajectory captured the DFT trajectory well indicating that the symmetric terms are the most important in the expression of model polarizability (Eq. 2 of the main paper). The trajectory of the models without the asymmetry terms show some deviation from the DFT trajectory, indicating that the asymmetry terms are the next most important after the symmetric terms. By contrast, a careful observation of the figure shows that the inclusion of m in the model has a weak effect because the trajectories calculated from conditions (a) and (c) are nearly identical. However, the importance of m has already been demonstrated in the main paper for large lattice parameter changes.

We then used those four sets of constants as extracted for the above four cases in order to calculate the Raman spectra of single domain of BTO thin film (cell size: 30×10×10) at 130 K. Fig. S3 shows the calculated Raman spectra for these four cases. For all cases, similar peak positions are obtained in the spectra. The impact of each terms on the intensity are also visible in the spectra.

BATIO₃ FIVE ATOMS CELL

Figs. S4, S5, S6 and S7 show the model polarizability (α_{xx} , α_{yy} and α_{zz}) trajectory along with that from DFT in case of five-atom BTO at 200 K, 300 K, 400 K and 600 K, respectively, as obtained from AIMD, DFT and model. All the model trajectories show good agreement

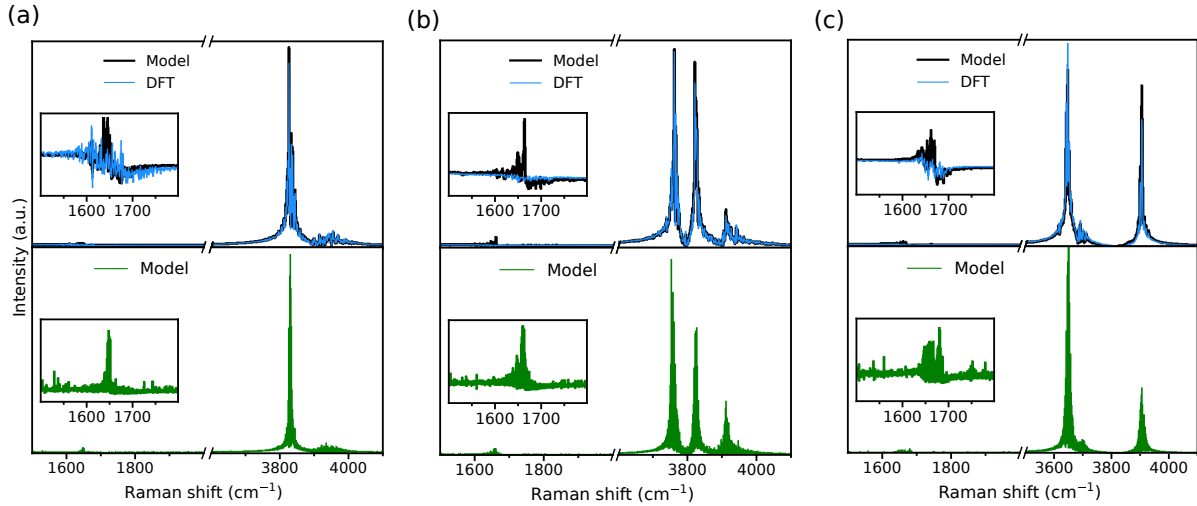


FIG. 1. (color online) Raman spectra of (a) H_2O : for short trajectory (top panel) and for long trajectory (bottom panel), (b) $(\text{H}_2\text{O})_2$: for short trajectory (top panel) and for long trajectory (bottom panel), (c) $(\text{H}_2\text{O})_3$: for short trajectory (top panel) and for long trajectory (bottom panel). Model spectra in blue and green. DFT spectra in filled red. Inset of each graph shows the spectra in the region of 1600 cm^{-1} .

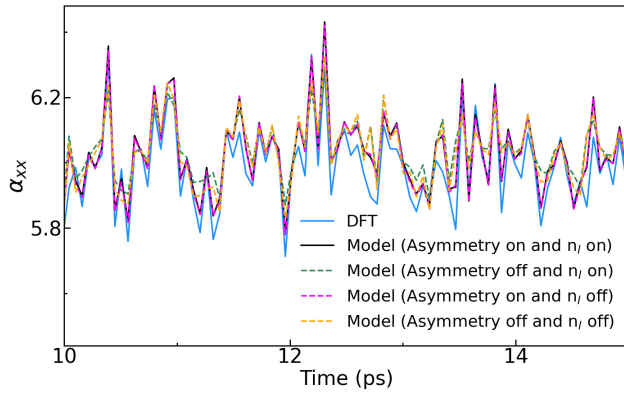


FIG. 2. (color online) Comparison of the polarizability (α_{xx}) trajectories from DFT, model (asymmetry on and m on), model (asymmetry off and m on), model (asymmetry on and m off) and model (asymmetry off and m off) for BTO (5 atom cell) at 300 K.

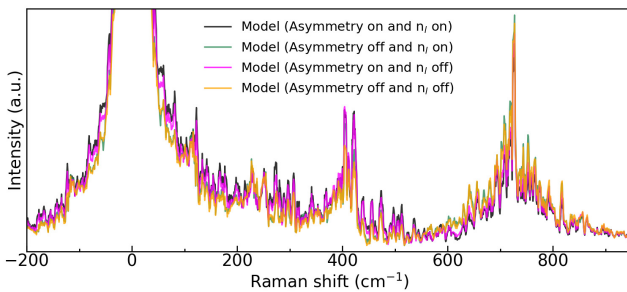


FIG. 3. (color online) Comparison of Raman spectra for single domain of BTO thin film (cell size: $30 \times 10 \times 10$) using the polarizability trajectory from the model (asymmetry on and m on), model (asymmetry off and m on), model (asymmetry on and m off) and model (asymmetry off and m off).

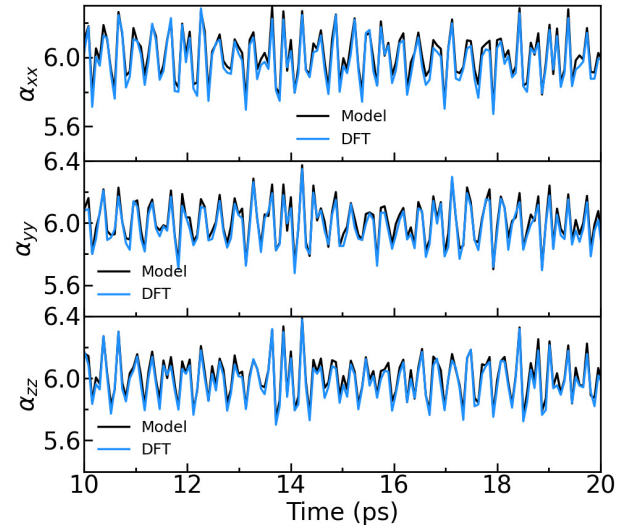


FIG. 4. (color online) Polarizability (α_{xx} (top panel), α_{yy} (middle panel) and α_{zz} (bottom panel)) trajectory from DFT and model of BTO at 200 K.

with the DFT results.

The Raman spectra at each temperature are also shown in Fig. S8. The Raman spectra were calculated using AIMD trajectory of up to 25 ps with a time step of 0.0014 ps.

BATIO₃ SINGLE DOMAIN AND POLYDOMAIN STATE CALCULATIONS

In Fig. S9, we present the BTO phases by showing the time evolution of Ti displacement for up to 300 ps at

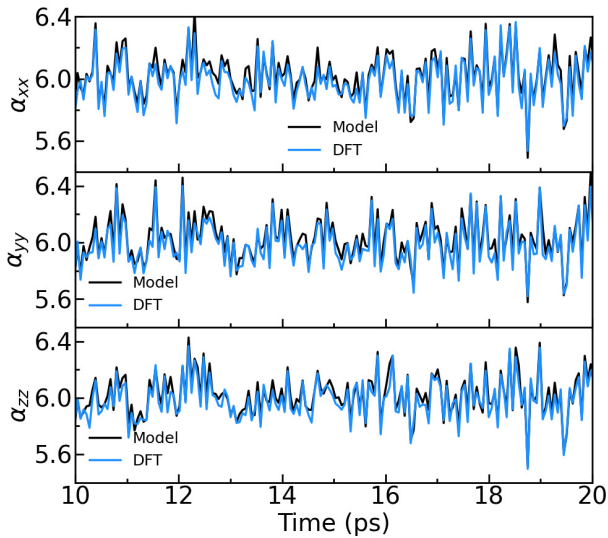


FIG. 5. (color online) Polarizability (α_{xx} (top panel), α_{yy} (middle panel) and α_{zz} (bottom panel)) trajectory from DFT and model of BTO at 300 K.

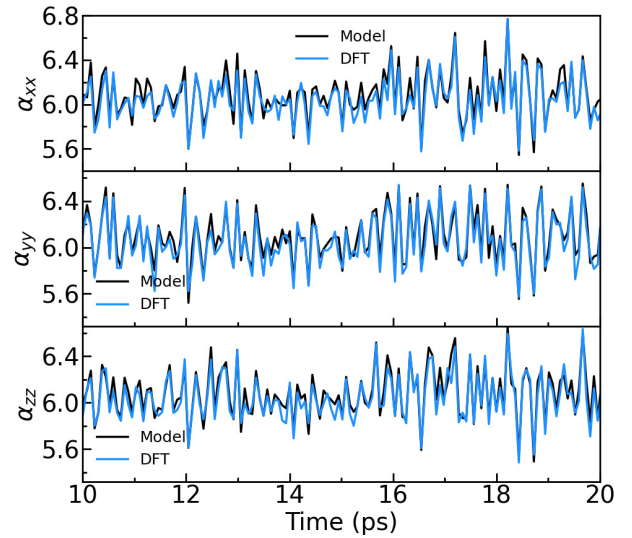


FIG. 7. (color online) Polarizability (α_{xx} (top panel), α_{yy} (middle panel) and α_{zz} (bottom panel)) trajectory from DFT and model of BTO at 600 K.

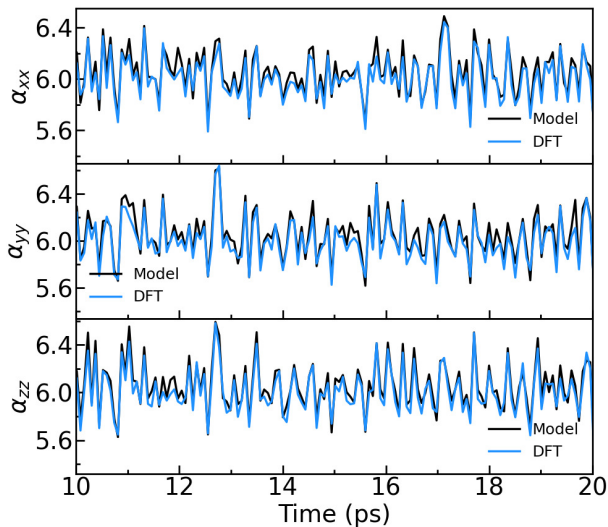


FIG. 6. (color online) Polarizability (α_{xx} (top panel), α_{yy} (middle panel) and α_{zz} (bottom panel)) trajectory from DFT and model of BTO at 400 K.

each temperature after molecular dynamics simulation on single-domain BTO with a $16 \times 16 \times 16$ cell. Figs. S9(a) and (b) are obtained from the simulations at 20 K and 50 K, respectively, which correspond to the rhombohedral phase of BTO. Fig. S9(c) is plotted for simulation temperature 92 K which shows the orthorhombic phase below 260 ps and rhombohedral phase above 270 ps. The molecular dynamics simulations at 110 K and 130 K captured the tetragonal phase as shown in Fig. S9(d) and (e), respectively. The cubic phase is obtained at 160 K as shown in Fig. S9(f). The Raman spectra of all of these phases have

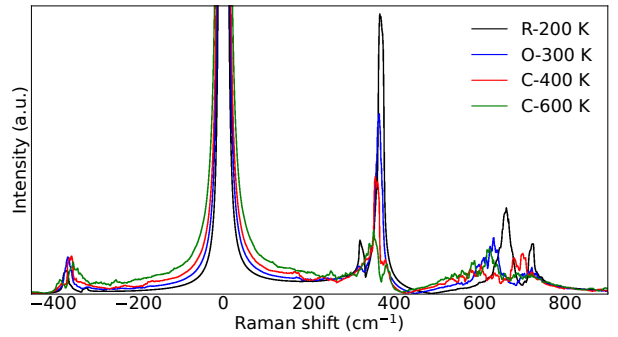


FIG. 8. (color online) Raman spectra of 5-atom BTO for different temperatures. The temperature along with the phases (R: rhombohedral, O: orthorhombic, C: cubic) are mentioned.

already been shown in the main paper. For the sake of completeness again we have shown the model Raman spectra along with the experimental Raman spectra in more details for the entire frequency range (see Fig. S10).

In Fig. S11, we represent the various domain structures of BTO that can be achieved in thin films as obtained from the classical molecular dynamics using a $120 \times 120 \times 6$ cell of BTO at 130 K. Figs. S11 (a), (b) and (c) show the single-domain, and 180° and aa or ac 90° domain structures of BTO, respectively. The 2D projection of the aa or ac domain wall structure is also shown in Fig. S11 (d).

CSPBBR₃

To demonstrate that the model is general and applicable to non-oxide systems, we apply it to the halide perovskite CPB. The values of the constants are presented in 'COMPUTATIONAL DETAILS' section. In Fig. S12 (a) we present the polarizability trajectory as calculated from model along with that from DFT for CPB at 400 K. Clearly, the model results reproduces the DFT results very well. Next, we compared the model spectra with the DFT-derived spectra for short trajectory and large time step as shown in Fig. S12 (b), confirming that this model can reproduce the Raman spectra of CPB.

CO₂ MOLECULE

The model Raman spectra of CO₂ at 300 K as calculated using AIMD trajectory for 64 ps is shown in Fig. S13.

EFFECT OF BaO₁₂ ON POLARIZABILITY OF BTO

In order to understand the contribution of BaO₁₂ polyhedra to the change in the polarizability and the dielectric constant, we have considered cubic centrosymmetric structure of BTO (5-atom cell) and calculated the dielectric constant for different displacements of Ba and Ti atoms along x -axis. Fig. S14(a) represents the evolution of ϵ_{xx} and ϵ_{yy} as a function of Ti displacement from its centrosymmetric position denoted by d_{Ti} for two positions of Ba ($d_{Ba} = 0.00$ and 0.08 Å, where d_{Ba} is the displacement of the Ba atom from its centrosymmetric position). Nearly parabolic dependence of ϵ_{xx} and ϵ_{yy} on d_{Ti} is observed. This indicates the importance of

the TiO₆ octahedra contribution to the polarizability of BTO. It is also observed that the two curves for different values of d_{Ba} are nearly degenerate, indicating the lower importance of the BaO₁₂ contribution to the polarizability of BTO. In Fig. S14(b), we plotted the variation of ϵ_{xx} and ϵ_{yy} as a function of d_{Ba} for two values of d_{Ti} . As expected, the change in the polarizability is much smaller in comparison to that for the Ti displacement. Therefore, we have neglected the effect of BaO₁₂ octahedra from the model of the polarizability for BTO.

* ilya.grinberg@biu.ac.il

- [1] P. Giannozzi, S. Baroni, N. Bonini, M. Calandra, R. Car, C. Cavazzoni, D. Ceresoli, G. L. Chiarotti, M. Cococcioni, I. Dabo, A. D. Corso, S. de Gironcoli, S. Fabris, G. Fratesi, R. Gebauer, U. Gerstmann, C. Gougoussis, A. Kokalj, M. Lazzeri, L. Martin-Samos, N. Marzari, F. Mauri, R. Mazzarello, S. Paolini, A. Pasquarello, L. Paulatto, C. Sbraccia, S. Scandolo, G. Sclauzero, A. P. Seitsonen, A. Smogunov, P. Umari, and R. M. Wentzcovitch, *Journal of Physics: Condensed Matter* **21**, 395502 (2009).
- [2] J. P. Perdew, A. Ruzsinszky, G. I. Csonka, O. A. Vydrov, G. E. Scuseria, L. A. Constantin, X. Zhou, and K. Burke, *Phys. Rev. Lett.* **100**, 136406 (2008).
- [3] V. Babin, G. R. Medders, and F. Paesani, *Journal of Chemical Theory and Computation* **10**, 1599 (2014).
- [4] P. Eastman, J. Swails, J. D. Chodera, R. T. McGibbon, Y. Zhao, K. A. Beauchamp, L.-P. Wang, A. C. Simmonett, M. P. Harrigan, C. D. Stern, R. P. Wiewiora, B. R. Brooks, and V. S. Pande, *bioRxiv* (2017), 10.1101/091801.
- [5] A. P. Thompson, H. M. Aktulga, R. Berger, D. S. Bolintineanu, W. M. Brown, P. S. Crozier, P. J. in 't Veld, A. Kohlmeyer, S. G. Moore, T. D. Nguyen, R. Shan, M. J. Stevens, J. Tranchida, C. Trott, and S. J. Plimpton, *Comp. Phys. Comm.* **271**, 108171 (2022).
- [6] Y. Qi, S. Liu, I. Grinberg, and A. M. Rappe, *Phys. Rev. B* **94**, 134308 (2016).

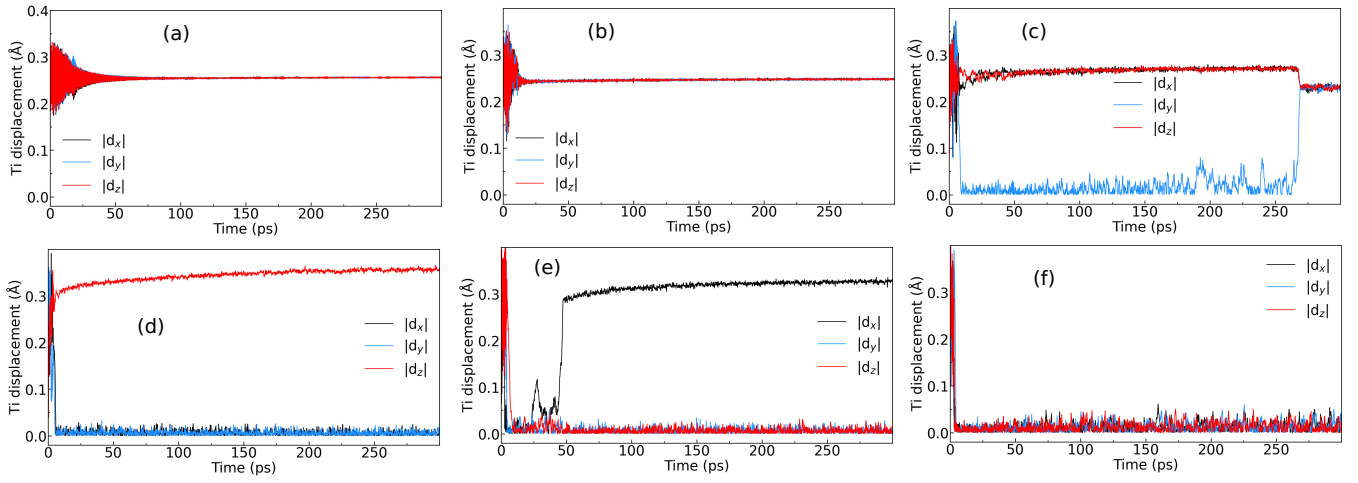


FIG. 9. (color online) Ti displacement (\AA) for up to 300 ps at temperatures of (a) 20 K (rhombohedral phase), (b) 50 K (rhombohedral phase), (c) 92 K (orthorhombic phase: up to 260 ps, rhombohedral phase: beyond 270 ps), (d) 110 K (tetragonal phase), (e) 130 K (tetragonal phase: above 50 ps) and (f) 160 K (cubic phase).

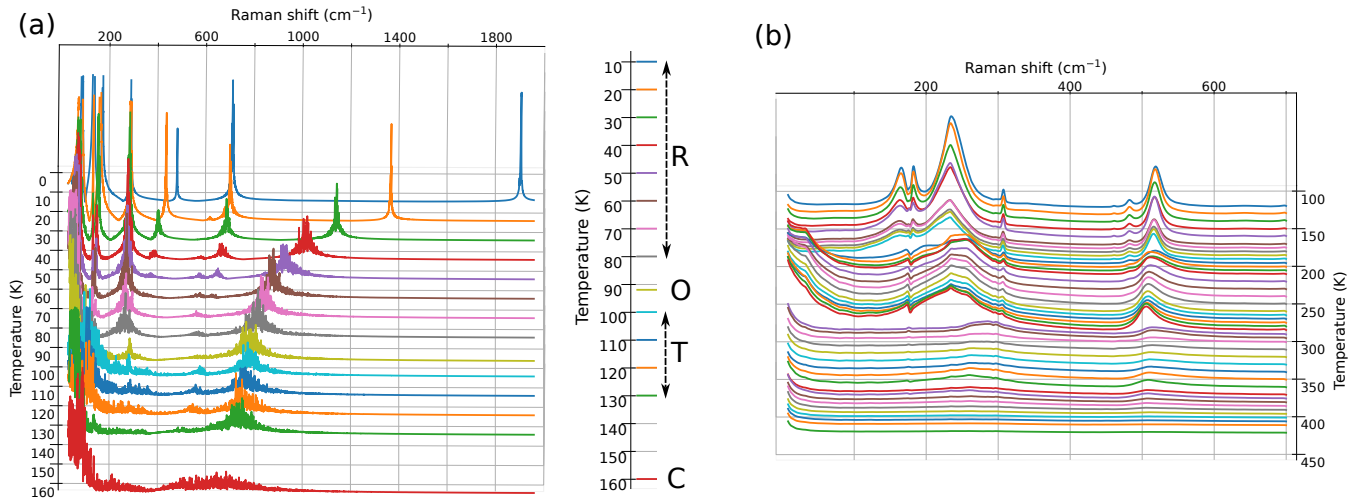


FIG. 10. (color online) Raman spectra of single-domain BTO for different temperatures as shown from (a) model and (b) experiment. R, O, T and C in the color bar represent the rhombohedral, orthorhombic, tetragonal and cubic phase for model.

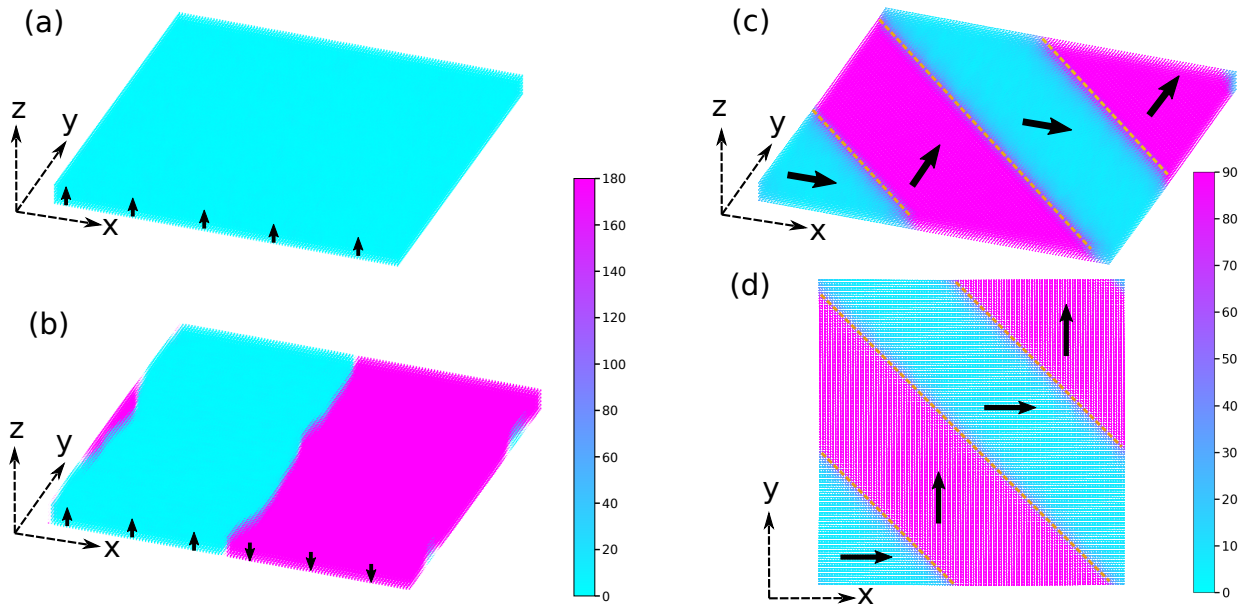


FIG. 11. (color online) (a) single domain, (b) 180° domain, (c) ac or aa 90° domain, (d) 2D projection of ac or aa 90° domain structure of BTO (cell size: $120 \times 120 \times 6$). The arrows (black) represent the directions of polarization in each domain. The orange dotted lines indicate the domain wall region in case of (c) and (d).

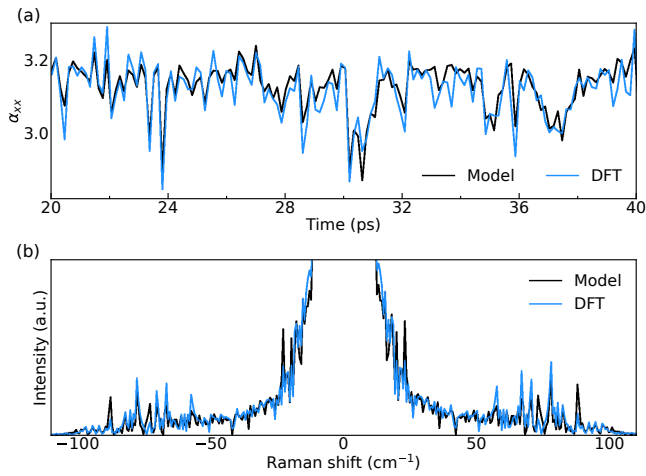


FIG. 12. (Color online) (a) Polarizability trajectory of CsPbBr_3 at 400 K using DFT and model. (b) Raman spectra CsPbBr_3 using the trajectory at 400 K.

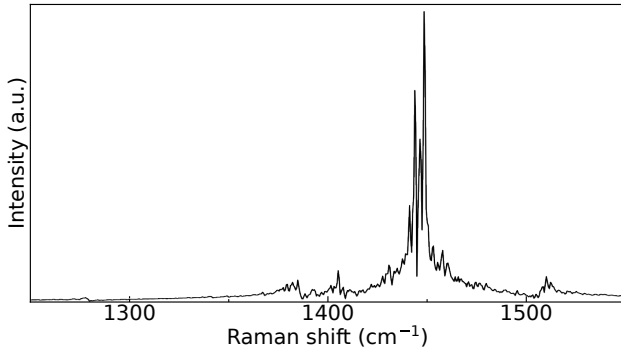


FIG. 13. (color online) Raman spectra of CO_2 at 300 K using the model polarizability trajectory.

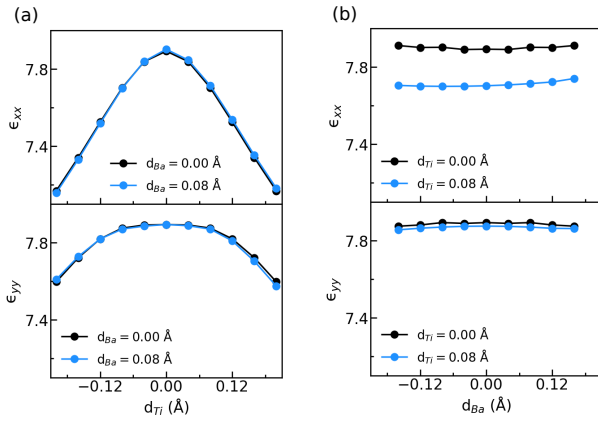


FIG. 14. (color online) ϵ_{xx} and ϵ_{yy} of BTO (5-atom cell), where d_{Ba} and d_{Ti} are the displacements of Ba and Ti atoms respectively along x direction from its centrosymmetric position denoted by $d_{Ba} = 0$ and $d_{Ti} = 0$. (a) ϵ_{xx} (first panel) and ϵ_{yy} (second panel) as a function of d_{Ti} for two values of d_{Ba} (0.00 and 0.08 Å). (b) ϵ_{xx} (first panel) and ϵ_{yy} (second panel) as a function of d_{Ba} for two values of d_{Ti} (0.00 and 0.08 Å).